Numerical simulation of CO$_2$ injection into deep saline aquifers

Ana González-Nicolás[1], Brent Cody[2], Domenico Baù[3]
Department of Civil and Environmental Engineering, Colorado State University, Fort Collins

Abstract. In the last two centuries, atmospheric concentrations of carbon dioxide (CO$_2$) have increased by about 35% as a result of anthropogenic emissions. To reduce these emissions, geologic Carbon Capture and Sequestration (CCS) has been introduced as an emerging technology. Current estimations report that deep saline formations account for approximately 60% of the total subsurface storage. Carbon geologic storage involves the injection of CO$_2$ in supercritical state into deep confined aquifers and can be modeled based upon the theory of two-phase flow in porous media. Supercritical CO$_2$ is less dense and less viscous than brine, which causes gravity override. The mass conservation equations for the two phases constitute a non-linear system of partial differential equations (PDE). In this work, MFLOW3D, a numerical finite-element model, is used to solve this non-linear system of PDE's and to test the simulation of CO$_2$ injection into a hypothetical and ideal confined aquifers. In MFLOW3D, the PDE's are discretized in space using linear three-dimensional finite elements in order to obtain a nonlinear system of ordinary differential equations. The temporal discretization is implemented via a finite difference backward-Euler scheme. The non-linearity is solved by using Newton-like iterative methods. Several scenarios are here simulated in order to analyze the effect of different factors on the accuracy of MFLOW3D results. These factors are: resolution and non regularity of finite element mesh, presence of subsurface heterogeneities, and lateral size of the domain. The reliability of simulations is checked for global accuracy in terms of the mass balance relative error for the injected CO$_2$. The numerical tests offer an important feedback on the capabilities and limitations of the adopted numerical approach.

1. Introduction

In the last two centuries, atmospheric concentrations of carbon dioxide have increased by about 35% as a result of increased anthropogenic emissions (Metz et al., 2005). To reduce carbon emissions, geologic CCS has been introduced as an emerging technology. The Intergovernmental Panel of Climate Change (IPCC) estimated storage capacity at a minimum of 1,678 GtCO$_2$ and potentially much higher, of which 60% are of deep saline formations (Price et al., 2008). Candidate storage formations include abandoned oil and natural gas reservoirs, un-mineable coal seams and deep saline aquifers (Bergman and Winter, 1995; Ruether, 1998).

Carbon geologic storage involves the injection of CO$_2$ in supercritical state into deep confined aquifers and can be modeled based upon the theory of two-phase flow in porous media. Supercritical CO$_2$ is less dense and less viscous than brine, which causes gravity override as well as possible viscous fingering. The mass conservation equations for the two phases constitute a non-linear system of partial differential equations (PDE).

The modeling of CO$_2$ injection in deep saline aquifers is a rather new subject of investigation. Different efforts to simulate this process have been conducted since there is a necessity of robust models. Van der Meer (1995), Pruess and Garcia (2002), Pruess et al. (2003), and Prevost et al. (2005) have all used idealized representations of the geology for

---

[1] e-mail: anagna@engr.colostate.edu
[2] e-mail: codybm@engr.colostate.edu
[3] e-mail: domenico.bau@colostate.edu

their studies of injection of CO_2 into deep formations. Pruess et al. (2004) and Class et al. (2009) evaluate different numerical codes with respect to their efficiency and accuracy in their ability to model the processes that take place when CO_2 is injected into a saline formation. In Class et al.(2009) the injection of CO_2 is simulated in the Johansen formation (Norway). Different boundary conditions, sensitivity with respect to vertical grid refinement, permeability/transmissibility data and the effect of residual gas saturations are considered in this study since these affect the distribution of the CO_2 plume. Birkholzer et al. (2009) evaluate the possible impact of industrial-scale CO_2 injection on regional multi-layered groundwater systems depending on different values of seal permeability.

These are some examples of the increasing number of research studies that have been published during the last fifteen years. In Schnaar and Digiulio (2009) a more detailed summary of modeling studies of CO_2 injection into subsurface is reported.

In this paper the accuracy of MFLOW3D in the modeling of CO_2 injection into a hypothetical and ideal confined aquifer is checked. MFLOW3D is used to solve the non-linear system of PDE's. These PDE's are discretized in space using linear three-dimensional finite elements (FE) in order to obtain a nonlinear system of ordinary differential equations (ODE). The temporal discretization is implemented via a finite difference backward-Euler scheme. The non-linearity is solved by using Newton-like iterative methods.

Several scenarios are presented where different factors are changed to analyze their effect on the accuracy of MFLOW3D results. These factors are: (1) resolution and non regularity of finite element mesh, (2) presence of subsurface heterogeneities, and (3) lateral size of the domain.

Presented below are the governing equations of two-phase flow in porous media and a brief summary of the numerical techniques used by MFLOW3D, followed by the numerical tests and results obtained. Finally the conclusions are presented.

2. Governing Equations for Two-Phase Flow in Porous Media

Carbon injection into deep saline aquifers involves two-phase flow in confined geological formations. If the two fluids are immiscible, no mass transfer between them occurs and the mass of each phase (denoted as α) is conserved. One of the phases has more attraction to the solid and wets the pore space more than the other. This phase is called the wetting phase (w), while the other phase is called the non-wetting phase (n), as its attraction to the solid phase is less.

In the case of injecting CO_2 into a deep saline aquifer, the wetting phase w is the brine (water saturated or nearly saturated with salt), while the non-wetting phase n is the super-critical CO_2. In two-phase flow, the pore volume is be occupied by two fluids. The porosity of each phase α, ϕ_α, corresponds to the fraction of bulk volume V that is occupied by that phase:

$$\phi_\alpha = \frac{V_\alpha}{V} \tag{1}$$

where V_α is the volume of phase α. Given that the pore volume V_v is fully occupied by the two phases, that is $V_{v=} V_w + V_n$. The total porosity is:

$$\phi = \phi_w + \phi_n \tag{2}$$

By defining, the saturation of each phase, S_α, as the fraction of pore volume $\varnothing \cdot V$ that is occupied by that phase, the porosity of the phase is given by:

$$\phi_\alpha = S_\alpha \cdot \phi \tag{3}$$

For two-phase flow, the range of either of the two phases can range from zero to one: $0 \le S_\alpha \le 1$. That is to say, each phase α can fill completely the space pore or be totally absent. Hence, when the pore space is filled by the different fluids the following relationship must hold (Chen et al., 2006):

$$S_n + S_w = 1 \tag{4}$$

Consequently, the saturation of the non-wetting phase can be defined as: $S_n = 1 - S_w$.

An important characteristic of multi-phase flow is that fluids not only interact with the solid phase, but also with each other. Because of the curvature and surface tension of the interface that exists between the two fluids and the solids, the pressure of the non-wetting phase is greater than in the wetting phase (Chen et al., 2006). This difference of pressure between the non-wetting and the wetting phase is called "capillary pressure", *Pc*, which is observed to be dependent upon water saturation (e.g., Brooks and Corey, 1964):

$$P_c(S_w) = P_n - P_w \tag{5}$$

For immiscible two-phase flow in porous media in isothermal conditions, the mass conservation equation for the phase α is (Helmig, 1997; Chen et al., 2006) expressed as:

$$\frac{\partial(\phi \cdot \rho_\alpha \cdot S_\alpha)}{\partial t} = -\nabla \cdot (\rho_\alpha \cdot \boldsymbol{v}_\alpha) + \boldsymbol{q}_\alpha \tag{6}$$

where: ρ_α is the fluid density, $\boldsymbol{v}_\alpha$ is the Darcy velocity and $\boldsymbol{q}_\alpha$ is the mass source/sink rate of the fluid phase, and t is the time. The Darcy velocity in terms of pressure and elevation is (Pinder and Gray, 2008):

$$\boldsymbol{v}_\alpha = -\frac{\rho_\alpha \cdot \boldsymbol{k}_\alpha}{\mu_\alpha} \cdot \nabla h_\alpha = -\frac{\boldsymbol{k}_\alpha}{\mu_\alpha}(\nabla P_\alpha - \rho_\alpha \boldsymbol{g} \cdot \nabla z) \tag{7}$$

where: $\boldsymbol{k}_\alpha$, μ_α, h_α, and P_α are the effective permeability, the dynamic viscosity, the potential head and the pressure for phase α, g is the gravity acceleration, and z is the elevation. In practice, the flow of each fluid interferes with the other. Thus the effective permeability of the generic phase α cannot exceed the absolute intrinsic permeability $\boldsymbol{k}_s$ of the porous medium.

The intrinsic permeability $\boldsymbol{k}_s$ is a property of the solid phase controlled by the porosity and the structure of the pores, and is typically expressed by a 3×3 tensor k_{ij}. If the coordinate axes are aligned with the principal directions of flow, all the off-diagonal elements of $\boldsymbol{k}_s$ are zero and the tensor becomes a diagonal tensor k_{ii}:

$$\boldsymbol{k}_s = \begin{bmatrix} k_{xx} & 0 & 0 \\ 0 & k_{yy} & 0 \\ 0 & 0 & k_{zz} \end{bmatrix} \tag{8}$$

If the porous medium is isotropic, not only the off-diagonal elements of $\boldsymbol{k}_s$ are zero but also the diagonal terms k_{ii} are all equal to k_s. When $S_\alpha = 1$, only the phase α is present and $\boldsymbol{k}_\alpha = \boldsymbol{k}_s$. If $S_\alpha \le 1$ the pore space accessible for phase α is lesser because of the presence of the other phase and $\boldsymbol{k}_\alpha < \boldsymbol{k}_s$. The relationship between $\boldsymbol{k}_\alpha$ and $\boldsymbol{k}_s$ may be expressed as (Pinder and Gray, 2008):

$$\boldsymbol{k}_\alpha = k_{r\alpha} \boldsymbol{k}_s \tag{9}$$

where: $k_{r\alpha}$ is the relative permeability, that is, the tendency of phase α to wet the porous medium. Since also the relative permeability $k_{r\alpha}$ is observed to be related to the water saturation (e.g., Brooks and Corey, 1964), then:

$$0 \le k_{r\alpha}(S_w) \le 1 \tag{10}$$

Substituting Equation (7) into Equation (6), and using Equation (4) and (5), the mass conservation equations for the wetting and non-wetting phases can be rewritten as:

(a)
$$\frac{\partial(\phi \cdot \rho_w \cdot S_w)}{\partial t} = \nabla\left[\frac{\rho_w}{\mu_w} k_w (\nabla P_w - \rho_w \cdot g \cdot \nabla z)\right] + q_w$$

(b)
$$\frac{\partial[\phi \cdot \rho_n \cdot (1\text{-}S_w)]}{\partial t} = \nabla\left[\frac{\rho_n}{\mu_n} \cdot k_n (\nabla P_w + \nabla P_c - \rho_n \cdot g \cdot \nabla z)\right] + q_n \tag{11}$$

In Equation (11b), the capillary pressure P_c can be expressed as a function of S_w using experimentally-derived analytic equations provided, for example, by Brooks and Corey (1964) and van Genuchten (1980). Brooks and Corey (1964) and van Genuchten (1980) also offer analytical expressions for the relative permeability relative to the water saturation S_w (Eq. 10). The Brooks-Corey capillary model is characterized by the following equations:

(a)
$$k_{rw}(S_w) = S_{we}^{(2+3/\zeta)/\zeta}$$

(b)
$$k_{rn}(S_w) = (1 - S_{we})(1 - S_{we}^{(2+\zeta)/\zeta}) \tag{12}$$

(c)
$$P_c(S_w) = P_d S_{we}^{-1/\zeta}$$

where: P_d is the pore entry pressure representing the lowest capillary pressure needed to displace the wetting phase by the non-wetting phase in a fully saturated medium; ζ is the sorting factor or pore distribution index which is related to the medium pore size distribution; and S_{we} is the effective water saturation, defined as:

$$S_{we} = \frac{S_w - S_{wi}}{1 - S_{wi}} \tag{13}$$

where S_{wi} is called "irreducible" (or residual) water saturation.

3. Numerical Code

In the numerical model MFLOW3D (Comerlati, et al. 2003; Comerlati, et al., 2005) the multi-phase flow problem is solved following the "P_w-S_w" approach derived in PDE's (11). MFLOW3D may include constitutive capillary curves $k_{rw}(S_w)$ and $P_c(S_w)$ such as those formulated by Brooks and Corey (1964) and van Genuchten (1980), as well as profiles arbitrarily specified using tabulated piecewise linear functions. In MFLOW3D, PDE's (11) are discretized in space using linear three-dimensional FE (tetrahedrons) to obtain a nonlinear system of ODE's having the following form:

$$\mathbf{H} \cdot x + \mathbf{M} \cdot \dot{x} + q = 0 \tag{14}$$

In (14), x is the vector of the unknown nodal water pressure (P_w) and saturation (S_w), $\dot{x}$ is the time derivative of x, $\mathbf{H}$ is the wetting and non-wetting stiffness matrix, $\mathbf{M}$ is the mass matrix, and q is a vector including source/sink terms and second-type (Neumann) boundary conditions.

In MFLOW3D, the temporal discretization is implemented via a finite difference (FD) backward-Euler scheme:

$$\left[\mathbf{H}(x)+\frac{\mathbf{M}(x)}{\Delta t}\right]_{(k+1)}\cdot x_{(k+1)} = \left[\frac{\mathbf{M}(x)}{\Delta t}\right]_{(k+1)}\cdot x_{(k)} - q_{(k+1)} \tag{15}$$

where: Δt is the time step, and (k) and $(k+1)$ indicate the previous and the current time level, respectively. Because of the intrinsic dependence of the matrices $\mathbf{H}$ and $\mathbf{M}$ on x, the ODE's of the system (15) are non-linear. Therefore, the system is solved using Newton-like iterative method. To do so, (15) is rewritten as:

$$\mathbf{f}[x_{(k+1)}] = \left[\mathbf{H}+\frac{\mathbf{M}}{\Delta t}\right]_{(k+1)}\cdot x_{(k+1)} - \left(\left[\frac{\mathbf{M}}{\Delta t}\right]_{(k+1)}\cdot x_{(k)} - \mathbf{q}_{(k+1)}\right) = \mathbf{A}\cdot x_{(k+1)} - \overline{\mathbf{q}} = \mathbf{0} \tag{16}$$

By applying a Taylor series expansion and rearranging, the following Newton iterative scheme is obtained for any iteration (r):

$$x_{(k+1)}^{(r+1)} = x_{(k+1)}^{(r)} - \mathbf{A}^{-1}\cdot \mathbf{f}\left[x_{(k+1)}^{(r)}\right] \tag{17}$$

Convergence is considered achieved when a prescribed norm of the vector $\mathbf{x}_{(k+1)}^{(r+1)} - \mathbf{x}_{(k+1)}^{(r)}$ satisfies the following tests:

$$\left\|\mathbf{p}_{w(k+1)}^{(r+1)} - \mathbf{p}_{w(k+1)}^{(r)}\right\| \le \tau_{p_w} \qquad\qquad \left\|\mathbf{S}_{w(k+1)}^{(r+1)} - \mathbf{S}_{w(k+1)}^{(r)}\right\| \le \tau_{S_w} \tag{18}$$

where τ_{p_w} and τ_{S_w} are pre-established tolerances for water pressure and water saturation, respectively.

4. Numerical Tests

Several preliminary injection scenarios have been simulated using the multiphase finite element code MFLOW3D.

The considered three-dimensional domain is a 100-m thick, 20km × 20km, horizontal, homogeneous and isotropic aquifer (see Figure 1a). The domain is characterized by impervious tops and bottoms. In each case, the bottom was located at a depth of -1500 m, and the formation was symmetrical with respect to the X and Y axes of the reference system. The injection system was modeled as a vertical fully-screened well located at the origin of the reference system, where a CO_2 injection rate of 80 kg/s was imposed (Figure 1).

In each simulation, all hypothetical aquifers at initial time were fully saturated with water and without any presence of CO_2. Also, all pressures were initially hydrostatically distributed. Given the conditions of symmetry, the aquifer model could be reduced (four times) to a domain subject to no-flow boundary conditions everywhere except: a) at the X=Y=0 vertical edge, where a constant CO_2 injection rate Q_{inj}=20 kg/s was imposed; b) on the lateral boundaries (opposite to the injection well) where the initial conditions were preserved (Eq. 19).

$$P_w(x,y,z;t) = \rho_w \cdot g \cdot |z| \quad \forall\, x,y,z:\ x\ or\ y = \pm5000\ m\ and\ \text{-}1500\ m \le z \le -1400\ m \tag{19}$$
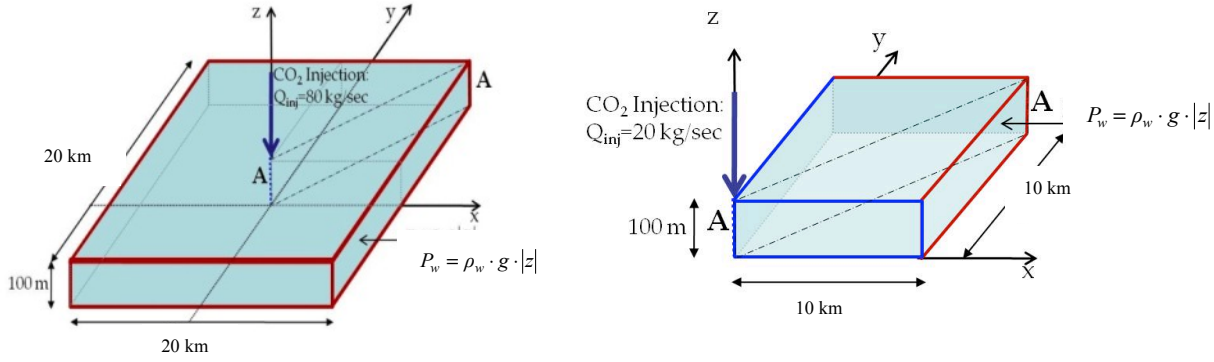
Figure 1. (a) Representation of the three-dimensional confined aquifer along with the boundary conditions considered in the simulation. (b) Given the conditions of symmetry the aquifer model may be reduced to a 10,000×10,000×100 (m×m×m) domain subject to no-flow boundary conditions everywhere except that on the lateral boundaries (outlined in red) where the initial undisturbed conditions are preserved. The vertical scale is exaggerated for clarity.

Figure 2 shows the capillary curves for the brine-supercritical CO_2-solid system that are used in the simulation tests to model the dependencies of the capillary pressure, and the relative permeabilities on the water saturation.
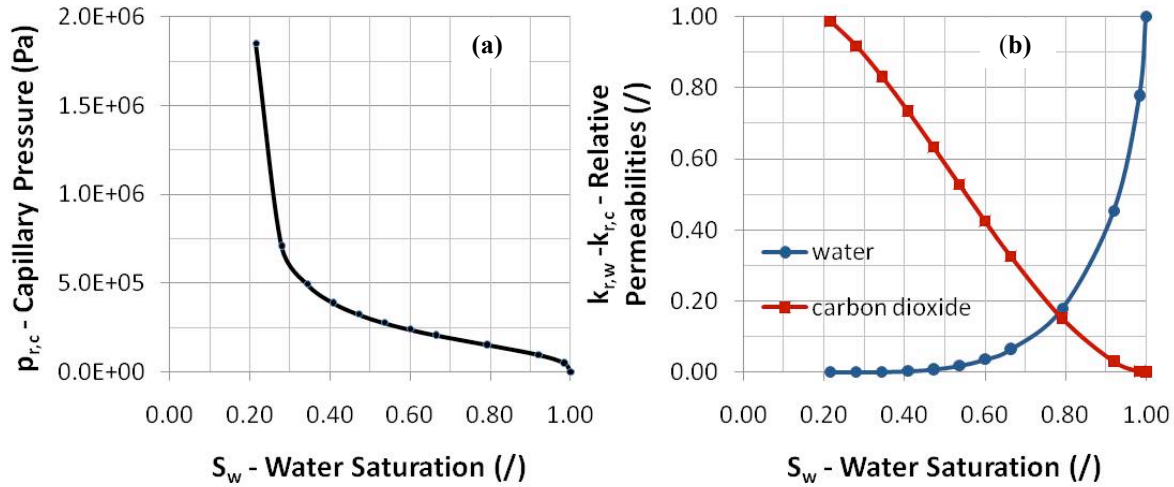
Figure 2. (a) Capillary pressure and (b) relative permeability curves for the brine-supercritical CO_2-solid system.

A summary of the formation's hydrogeological parameters is provided in Table 1. Although many of these parameters remain constant throughout all scenarios, domain size, grid composition, and aquitard permeability are varied in an attempt to investigate effects on MFLOW3D results by the given four investigated factors.

Domain dimensions ranged between 2,500 m and 15,000 m along the X and Y axes and between 100 m and 210 m along the Z axis. Grid block dimensions ranged between 50 m and 500 m along the X and Y axes and between 0.1 m and 25 m along the Z axis. Meshes contained between 2,205 and 132,613 nodes and between 9,600 and 720,000 elements. For the two-layer subsurface heterogeneity test aquitard permeabilities ranged between 10^{-16} m^2 and 10^{-25} m^2. For the sake of the discussion only some plots of representative results are presented. All the figures are at time 30 years.

Table 1. Constant hydrogeological properties.

Property	Symbol	Value (unit)
Porosity:	ϕ	0.3 (/)
Permeability:	k_s	1.0×10^{-13} m^2
Water Density:	ρ_w	1000 kg/m^3
CO$_2$ Density:	ρ_n	600 kg/m^3
Specific Elastic Storage:	S_S	2×10^{-6} m^{-1}
Water Viscosity:	μ_w	3.9×10^{-4} kg/(m·s)
CO$_2$ Viscosity:	μ_n	2.5×10^{-5} kg/(m·s)
Gravity:	g	9.81 m/s^2
Injection Rate:	Q_{inj}	20 kg/s
Time of injection:	t	30 years

Additionally, each simulation is checked for global accuracy by finding the maximum the mass balance relative error for CO$_2$ (Eq. 20). Most of the simulations have acceptable maximum relative error values (10^{-8} – 10^{-6}), and were deemed acceptable.

$$\max \theta_{r,CO_2}(t) = \max \left\{ \left| \frac{Q_{CO_2} \cdot t - \int_{\Omega} \varphi \cdot S_n(x,y,z;t) \cdot dV}{Q_{CO_2} \cdot t} \right| \right\} \tag{20}$$

4.1. Effects of Grid Resolution on Numerical Results

Four simulations with an extension of 10,000 m x 10,000 m are used to determine how grid refinement affects MFLOW3D results. In three simulations the horizontal grid block size was altered (50 m x 50 m, 100 m x 100 m, 500 m x 500 m) while the vertical grid block size was kept constant at 25 m. Another simulation had a horizontal grid block size of 100 m x 100 m while the vertical grid block dimension was lowered to 10 m. The finer meshes resulted in smoother contours lines for all plots (Figure 3 to Figure 6).

Interestingly, the courser grids produce the same general plume shape as finer, more costly meshes. In fact, there is very little difference between the outputs, however, the most refined simulation required 41% more computer time than the least refined simulation. Although comparatively fast, simulation with grid block size 500 m x 500 m x 25 m produced rough contour lines (Figure 5). The vertical grid size refinement greatly affected the smoothness of the CO$_2$ saturation contours in the RZ plane contour plot but did not seem to affect any of the other corresponding output plots.

In this case, the water pressure distribution and over-pressure plots (not presented in this paper) look very similar, indicating that grid size does not greatly affect water pressure contours. This is most likely resulting from the changes in water pressure throughout the domain being less sharp than changes in CO$_2$ saturation; hence, relatively small changes in grid block size do not affect contour line location.
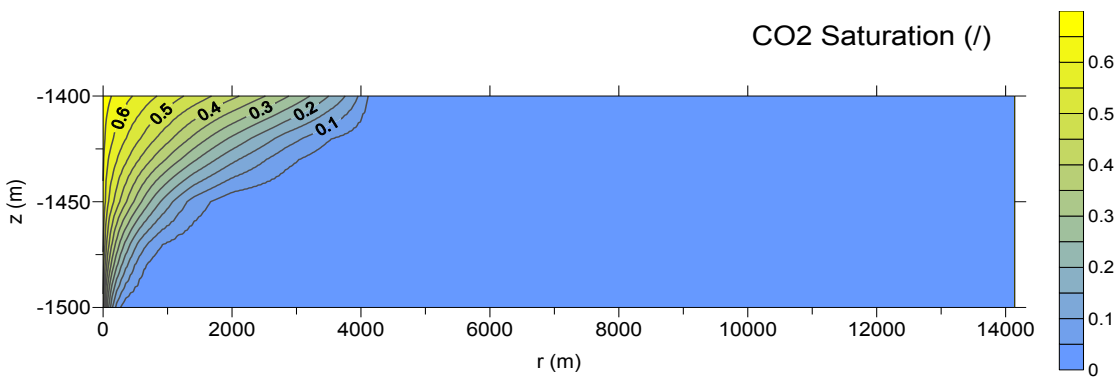
Figure 3. CO$_2$ saturation in the RZ plane for grid block size 50 m x 50 m x 25 m.
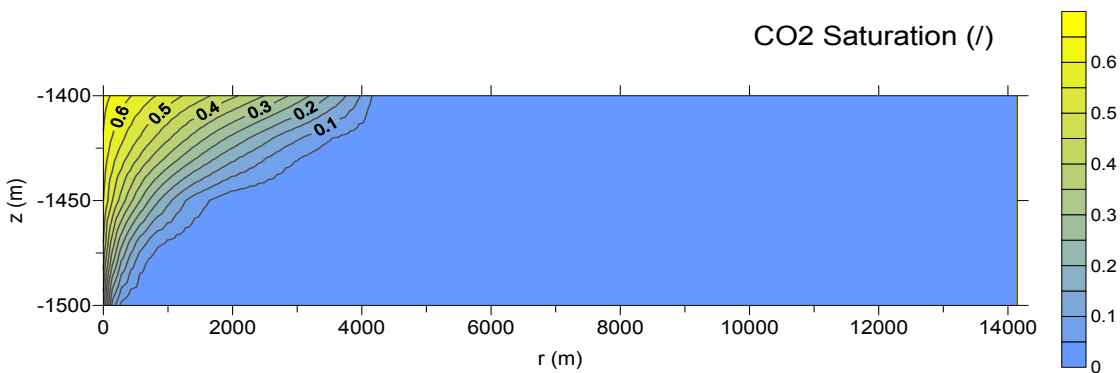

Figure 4. CO$_2$ saturation in the RZ plane for block size 100 m x 100 m x 25 m.
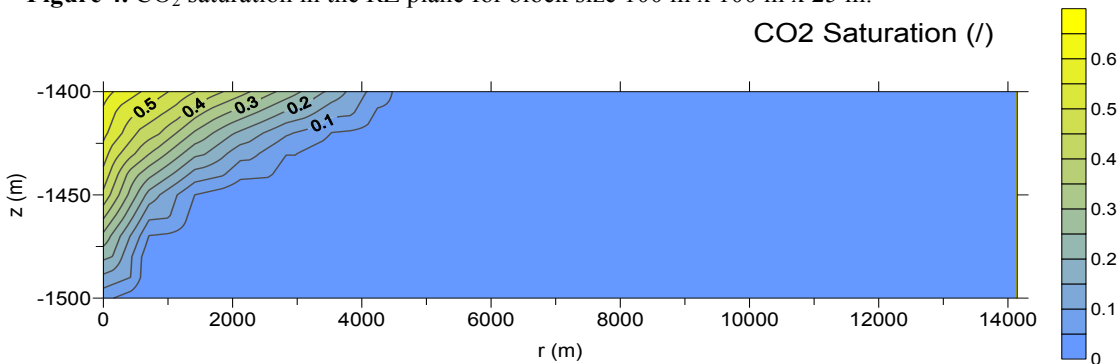

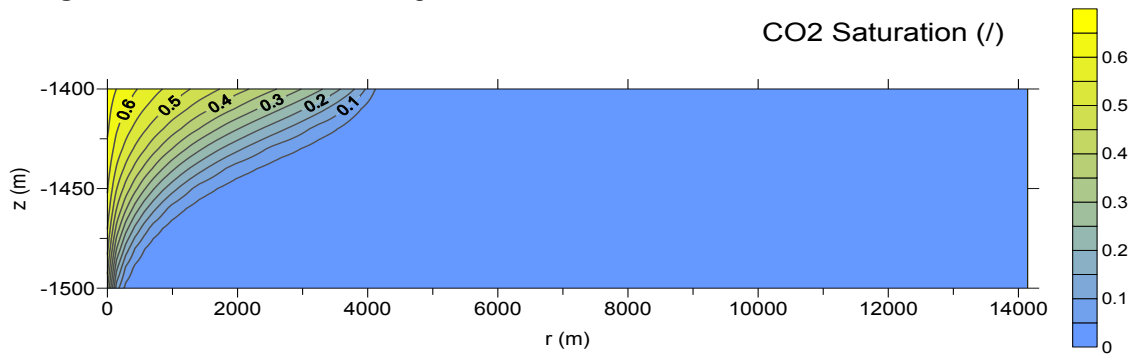**Figure 5.** CO$_2$ saturation in the RZ plane for block size 500 m x 500 m x 25 m.

Figure 6. CO$_2$ saturation in the RZ plane for block size 100 m x 100 m x 10 m.

4.2. Effects of Non-Regular Grids on Numerical Results

This section explores the use of non-regular grids with the primary purpose of achieving greater solution accuracy in near the injection well while maintaining similar computational costs. This is accomplished by using smaller elements closer to the injection location and larger elements at far distances while using the same number of nodes and elements (Figure 7).
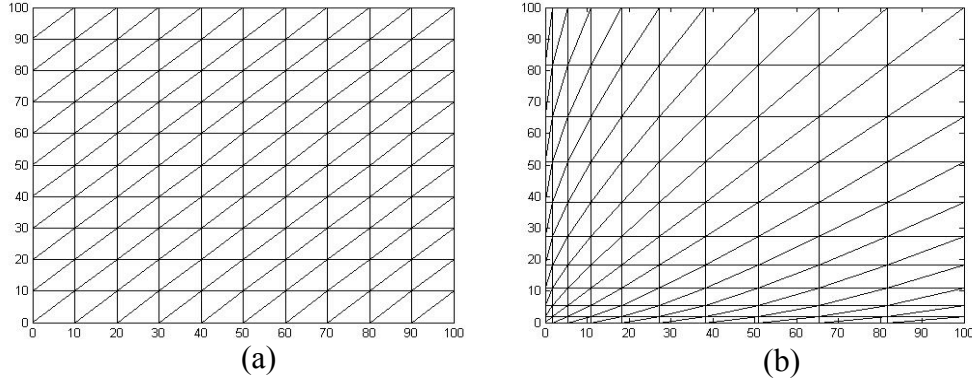
Figure 7. XY Plane View of (a) a regular grid sample (ratio 1/1) and (b) an irregular grid sample (ratio 1/10). Both have the same number of nodes and elements.

To explore effects of grid irregularity, all parameters were kept constant in each simulation except the size ratio between the first and last element along the X and Y axis. Ratios of 1/5, 1/10, 1/25, 1/50, 1/100 and 1/1000 are applied. The extent of the domain is 10,000 m x 10,000 m.

Results for ratios 1/5 and 1/50 are presented below (Figure 8 and 9). Simulation with grid block size 100 m x 100 m x25 m ratio 1/1 (Figure 4) produces a nearly identical output plot to the first four ratios.
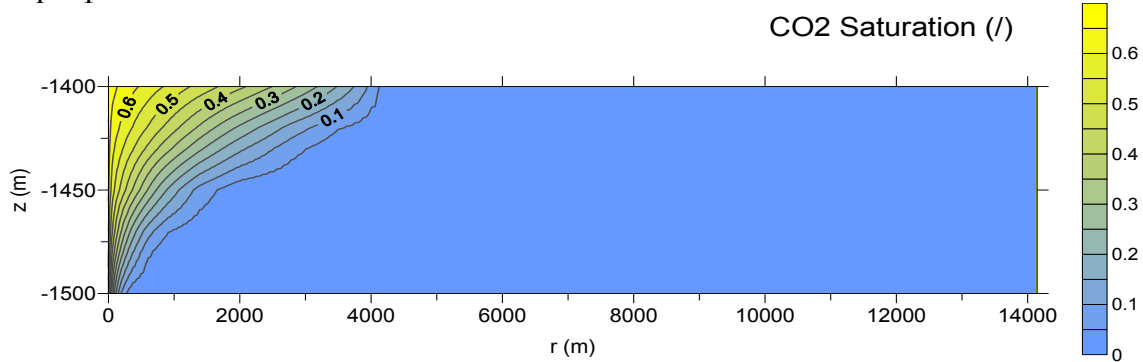

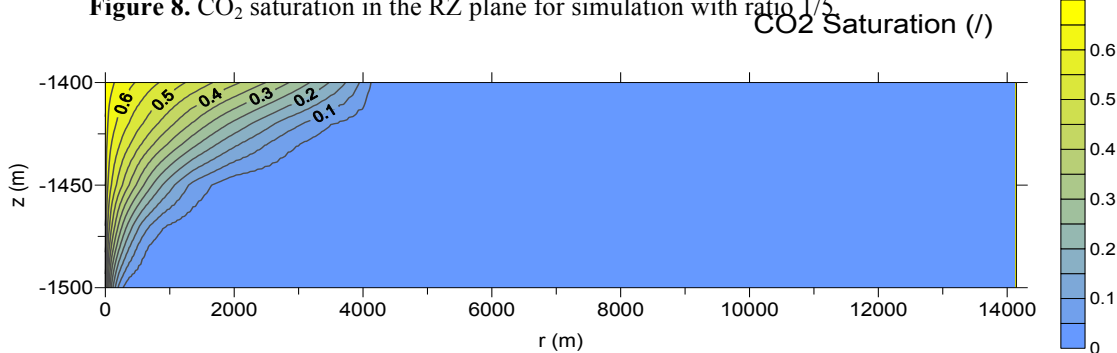**Figure 8.** CO_2 saturation in the RZ plane for simulation with ratio 1/5.

Figure 9. CO_2 saturation in the RZ plane for simulation with ratio 1/50.

These similarities between contour plots are most likely a result of the high level of discretization used for the meshes (51,005 nodes and 240,000 elements). With closer inspection, the non-regular meshes were found to produce much smoother contours and higher CO_2 saturations within approximately 300 m of the injection well. Simulations with ratios 1/100 and 1/1000 produced unacceptable relative error of the mass balance (2.3 x 10^{79} and 1.5 x 10^{174} respectively). This finding indicates that MFLOW3D is unable to process solutions using highly non-regular grids (i.e. ratios $\geq$ 100).

4.3. Effects of Subsurface Heterogeneities on Numerical Results

A hypothetical three layer system having a horizontal domain extent of 10,000m x 10,000m was simulated with the intent of analyzing subsurface heterogeneities. The system is composed of identical lower and upper aquifers separated by an aquitard. The aquifers are both 100 m thick, each having four 25 m vertical mesh layers and a permeability of 10^{-13} m^2. The aquitard is 10 m thick with vertical mesh layers of 0.1 m, 4.9 m, 4.9 m, and 0.1 m from bottom to top. Both the aquifers and the aquitard have a horizontal grid block size of 100 m x 100 m. CO_2 is injected into the lower aquifer at a rate of 20 kg/s. Two different aquitard permeabilities are applied: 10^{-19} m^2 and 10^{-25} m^2. This is the only parameter that changes between the two simulations.
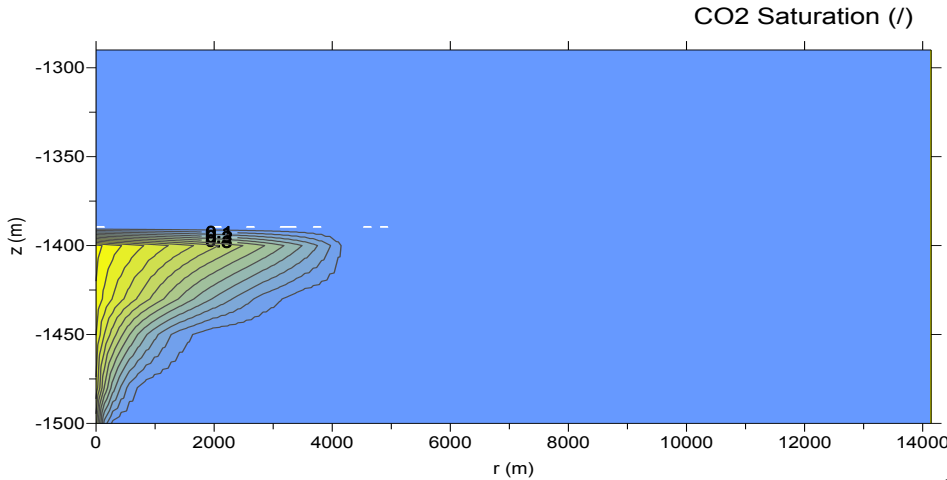

Figure 10. CO_2 saturation in the RZ plane for simulation with aquitard permeability of $10^{-19}m^2$.
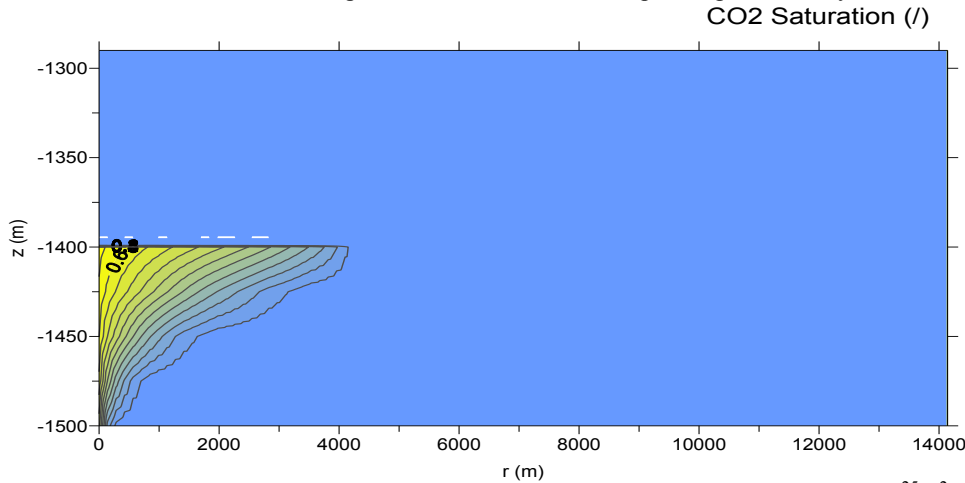

Figure 11. CO_2 saturation in the RZ plane for simulation aquitard permeability of $10^{-25}m^2$.

As expected, the CO_2 plume has a greater infiltration into the aquitard having the higher permeability (Figure 10 and 11). It is interesting to note that after 30 years the CO_2 plume is does not infiltrate the upper aquifer in either case. The CO_2 plume in the lower aquifer extends to the same depth and looks very similar for both cases. The greatest CO_2 concentrations in both simulation's aquifer and aquitard are closest to the injection well.

4.4. Effects of Varying Prescribed Lateral Boundary Conditions on Numerical Results

The horizontal domain sizes were altered to investigate effects of changing the lateral boundary distance on MFLOW3D results. The grid block size remained constant at 100m x 100m x 25m while the horizontal domain sizes are 2500 m, 5,000 m, 10,000 m, and 15,000 m. The two fronts of interest in this problem are the CO_2 plume and the water pressure pulse. The CO_2 plume is found to consistently grow to a radial distance of approximately 4100 m at the top of the aquifer ($z = -1400$ m) (Figure 13 and 15).

When the domain was set below this distance (as in the scenario of domain 2,500 m x 2,500 m) the plume collided with the outer boundary, rendering the solution invalid (Figure 12).
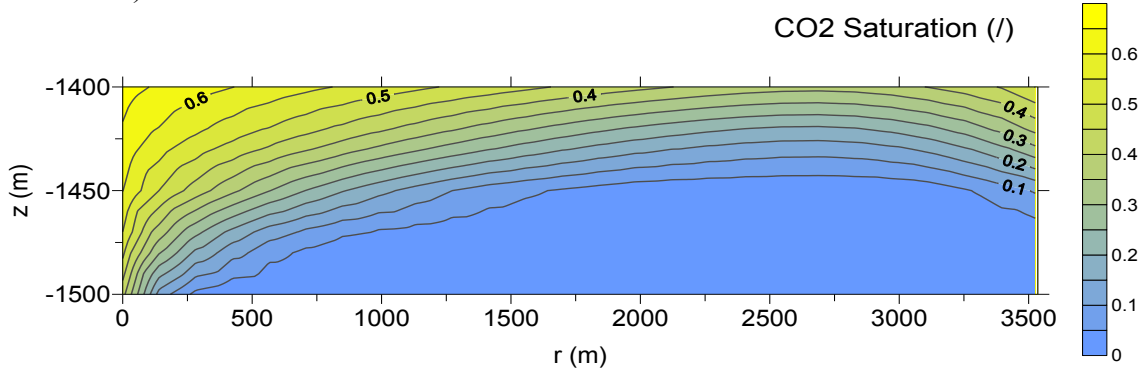

Figure 12. CO_2 saturation in the RZ plane for simulation with domain 2,500 m x 2,500 m.
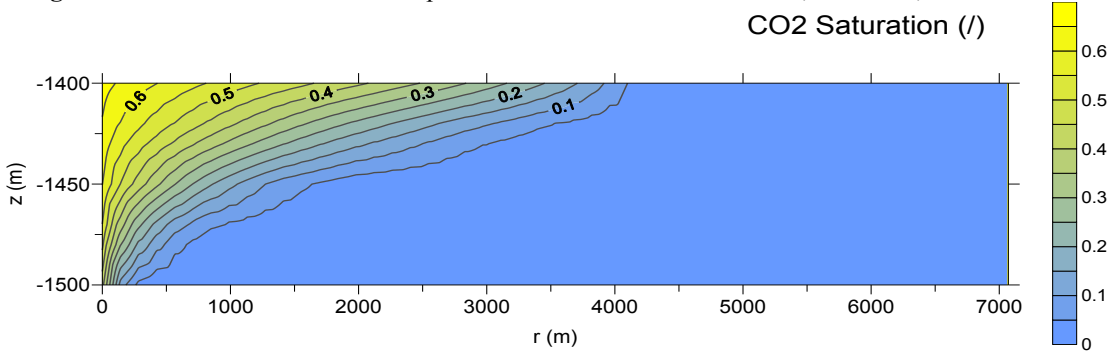

Figure 13. CO_2 saturation in the RZ plane for simulation with domain 5,000 m x 5,000 m.

The water pressure pulse seems to expand much further than originally believed and enlarges with an increasing outer boundary (Figure 16 and 17). Also, the pressure near the injection well increases with an increasing horizontal boundary. Further testing is needed in this area to determine the true extent of the pressure pulse at time 30 years.
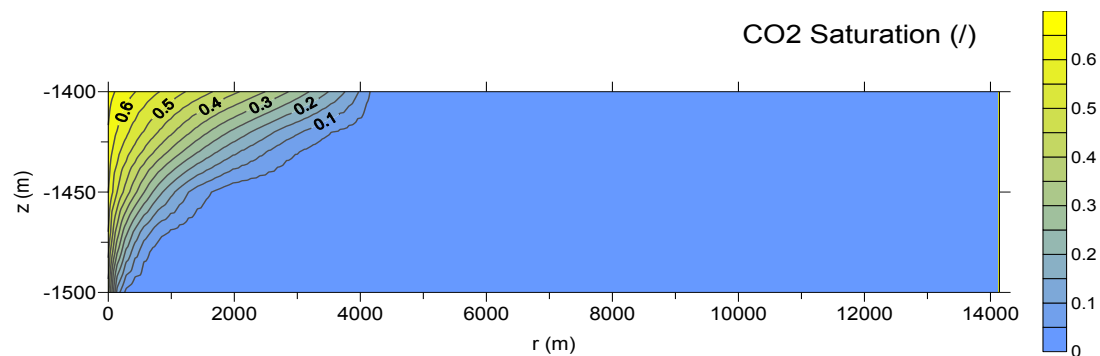
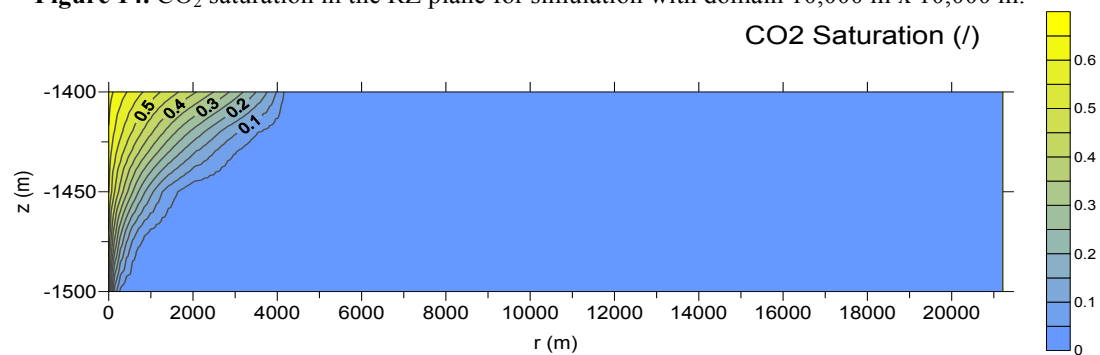**Figure 14.** CO$_2$ saturation in the RZ plane for simulation with domain 10,000 m x 10,000 m.

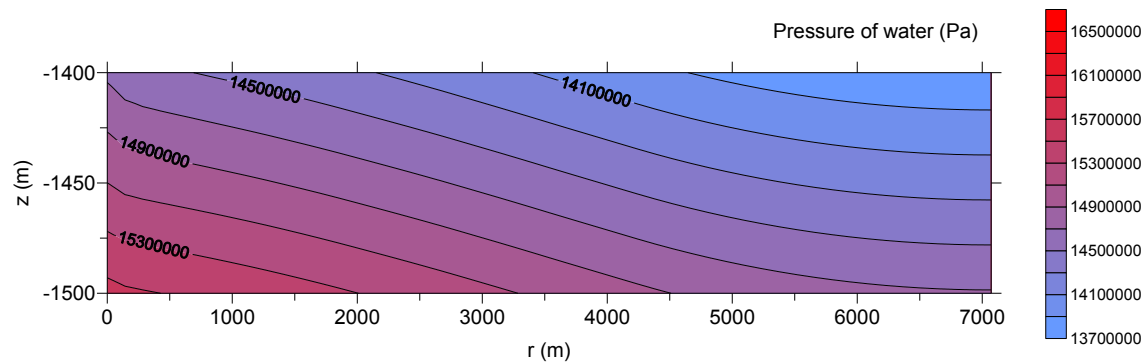**Figure 15.** CO$_2$ saturation in the RZ plane for simulation with domain 15,000 m x 15,000 m.

Figure 16. Water pressure in the RZ plane for simulation with domain 5,000 m x 5,000 m.
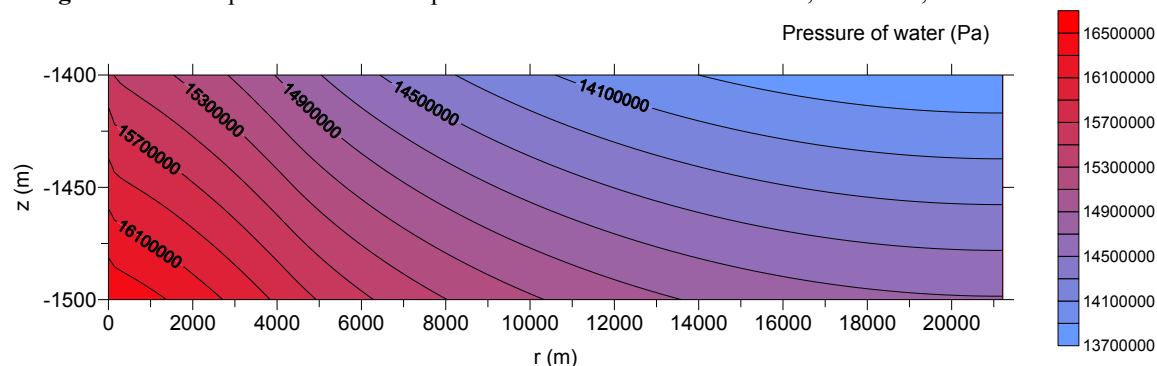
Figure 17. Water pressure in the RZ plane for simulation with domain 15,000 m x 15,000 m.

5. Conclusion

Fifteen different scenarios have been simulated using the FE multi-phase flow model MFLOW3D with the intent of understanding how grid resolution, grid regularity, subsurface heterogeneities, and imposed lateral boundary conditions affect MFLOW3D results.

The scenarios simulated to date provide insight into multiphase flow and MFLOW3D's limitations. A relatively small amount of mesh refinement adds computer time but does not alter the general plume shape. Mesh refinement does, however, give more accurate solutions around the injection well where higher pressures are observed. Non-regular grids seem to be effective in reducing computational time while maintaining near-well accuracy; however, MFLOW3D is unable to handle large element size variations. To model subsurface heterogeneities, two tri-layer simulations have been conducted which provided a preliminary insight into CO_2 migration out of an aquifer into semi-permeable cap rock. Lateral boundary distances must be larger than the CO_2 plume extent to provide acceptable results. Further tests are necessary to determine the pressure front extent and how it affects the CO_2 plume migration. The numerical tests performed to date present significant feedback on the capabilities and limitations of the implemented numerical approach.

References

Bergman, P.D. and E.M. Winter, 1995: Disposal of carbon dioxide in aquifer in the U.S. Energy Conversion Management, **36**: 523-526.

Birkholzer, J.T., Q. Zhou, C.-F. Tsang, 2009: Large-scale impact of CO_2 storage in deep saline aquifers: A sensitivity study on pressure response in stratified systems. International Journal of Greenhouse Gas Control, **3**: 181-194.

Brooks R.H. and A.T. Corey, 1964: Hydraulic properties of porous media. Hydrology Paper 3, Colorado State University, Fort Collins, CO.

Chen Z., Huan G. and Ma Y., 2006: Computational Methods for Multiphase Flows in Porous Media, *SIAM - Society for Industrial and Applied Mathematics*, 549 pp.

Class, H., A. Ebigbo, R. Helmig, H.K. Dahle, J.M. Nordbotten, M.A. Celia, P. Audigane, M. Darcis, J. Ennis-King, Y. Fan, B. Flemisch, S.E. Gasda, M. Jin, S. Krug, D. Labreger, A. Naderi Beni, R.J. Pawar, A. Sbai, S.G. Thomas, L. Trenty and L. Wei, 2009: A benchmark study on problems related to CO_2 storage in geologic formations. *Computational Geosciences*, **13**: 409-434.

Comerlati, A., G. Pini and G. Gambolati, 2005: Projection and partitioned solution for two-phase flow problems. *International Journal for numerical methods in fluids*, **49**: 1329-1346.

Comerlati, A., M. Ferronato, G. Gambolati, M. Putti and P. Teatini, 2003: Upward migration of anthropogenic CO_2 and vertical finite element mesh resolution in a layered sedimentary basin.

Helmig, R., 1997: Multiphase Flow and transport processes in the subsurface. Springer, Berlin, Germany, 367 pp.

Metz, B., O. Davidson, H.C. de Coninck, L.A. Meyer, Eds., 2005: IPCC Special Report on Carbon Dioxide Capture and Storage. Cambridge University Press: New York.

Pinder, G.F. and W.G. Gray, 2008: Essentials of multiphase flow and transport in porous media. Wiley, Hoboken, N.J.

Prevost, J.H., R. Fuller, A.S. Altevogt, R. Bruant and G.Scherer, 2005: Numerical Modeling of Carbon Dioxide injection and transport in deep saline aquifers. Greenhouse Gas Control Technologies, Volume II, 2189-2193.

Price J., S. McElligott, I. Price and B. Smith, 2008: Carbon Capture and Storage: Meeting the Challenge of climate change. IEA Greenhouse Gas R&D Programme. www.ieagreen.org.uk

Pruess, K. and J. Garcia, 2002: Multiphase flow dynamics during CO_2 injection into saline aquifers. *Environ. Geol.*, **42**, 282–295.

Pruess, K., J. Garcia, T. Kovscek, C. Oldenburg, J. Rutqvist, C. Steefel and T. Xu, 2004: Code intercomparison builds confidence in numerical simulation models for geologic disposal of CO_2. *Energy*, **29**, 1431–1444.

Pruess, K., T.F. Xu, J. Apps and J. Garcia, 2003: Numerical modeling of aquifer disposal of CO_2. *SPE J.*, **8**, 49–60..

Ruether, J.A., 1998: FETC Programs for Reducing Greenhouse Gas Emissions: Technical report, U.S. Department of Energy, Federal Energy Technology Center, Morgantown, WV.

Schnaar, G. and D.C. Digiulio,. 2009: Computational Modeling of the Geologic Sequestration of Carbon Dioxide. *Vadose Zone Journ,,l* **8**, No. 2: 389-403.

Van der Meer, L.G.H., 1995: The CO_2 storage efficiency of aquifers, *Energy Conservation and Management*, **36**(6-9), 513-518.

Van Genuchten, M.Th., 1980: A closed-form equation for predicting the hydraulic conductivity of unsaturated soils. Soil Science Society of America Journal, **44** (5): 892-898.